Structural, electronic, optical, elastic properties and Born effective charges of monoclinic HfO_2 from first-principles calculations*

Liu Qi-Jun(刘其军)[a)†], Zhang Ning-Chao(张宁超)[a)], Liu Fu-Sheng(刘福生)[a)], and Liu Zheng-Tang(刘正堂)[b)]

[a)] *Bond and Band Engineering Group, Institute of High Temperature and High Pressure Physics, School of Physical Science and Technology, Southwest Jiaotong University, Chengdu* 610031, *China*

[b)] *State Key Laboratory of Solidification Processing, School of Materials Science and Engineering, Northwestern Polytechnical University, Xi'an* 710072, *China*

(Received 30 July 2013; revised manuscript received 27 September 2013; published online 10 February 2014)

First-principles calculations of structural, electronic, optical, elastic, mechanical properties, and Born effective charges of monoclinic HfO_2 are performed with the plane-wave pseudopotential technique based on the density-functional theory. The calculated structural properties are consistent with the previous theoretical and experimental results. The electronic structure reveals that monoclinic HfO_2 has an indirect band gap. The analyses of density of states and Mulliken charges show mainly covalent nature in Hf-O bonds. Optical properties, including the dielectric function, refractive index, extinction coefficient, reflectivity, absorption coefficient, loss function, and optical conductivity each as a function of photon energy are calculated and show an optical anisotropy. Moreover, the independent elastic constants, bulk modulus, shear modulus, Young's modulus, Poisson's ratio, compressibility, Lamé constant, sound velocity, Debye temperature, and Born effective charges of monoclinic HfO_2 are obtained, which may help to understand monoclinic HfO_2 for future work.

Keywords: density-functional theory, optical properties, elastic constants, monoclinic HfO_2

PACS: 71.15.Mb, 71.22.+i, 62.20.dq **DOI:** 10.1088/1674-1056/23/4/047101

1. Introduction

Hafnia (HfO_2) is a technologically important compound that has been used as gate dielectrics,[1–5] ceramics,[6–8] interference filters,[9] optical coatings,[10] protective layer,[11] and superhard and refractory materials[12,13] due to its high dielectric constant, large band gap, sufficient band offsets, good thermal and interface stability in contact with Si, good reliability and compatibility with processing steps,[14–18] high refractive index,[9,10] high bulk modulus, and melting point.[12,19,20] Under normal pressure, HfO_2 crystallizes in three polymorphs:[19–22] a low temperature monoclinic phase (C_{2h}^5 or $P2_1/c$), a tetragonal phase (D_{4h}^{15} or $P4_2/nmc$) as the temperature increases, and finally a cubic phase (O_h^5 or $Fm3m$). Moreover, high-pressure phases, such as orthorhombic ($Pbca$ or D_{2h}^{15}) and orthorhombic ($Pnma$ or D_{2h}^{16}),[23–25] and other phases, such as modified fluorite phase ($Pa3$ or T_h^6),[20] amorphous phase,[18,26] have been reported.

As a gate dielectric to replace SiO_2 in metal–oxide–semiconductor field-effect transistor (MOSFET), a systematic investigation of the physical and chemical properties of HfO_2 in thin-film (surface and interface) is greatly desired. HfO_2 films have been grown by atomic layer deposition (ALD),[2,10,27,28] electron beam evaporation (e-beam),[2,29] reactive vacuum evaporation,[9] radio-frequency (rf) magnetron sputtering,[11,15] remote plasma-assisted chemical vapor deposition (RPECVD),[30] etc., and their structural, electrical, optical, thermo-mechanical, surface and interfacial properties have been studied. However, some properties, surface and interfacial properties in particular, are not well understood by experiments. This problem can be solved by theoretical calculations based on first-principles; for example, cubic HfO_2 surfaces with VASP code,[31] tetragonal HfO_2 (001) surface with CASTEP code,[32] Si(001)/HfO_2 interface,[33] HfO_2/interlayer and interlayer/Si interfaces,[34] HfO_2/SiO_2/Si interface,[35] and HfO_2/GaAs interface[36] with VASP code. Of course, an all-around study of bulk properties is also important to HfO_2 dielectric, which has been addressed experimentally[6,8,14,23,37] and theoretically.[38–44] Its dielectric constants have been reported to be 25,[14] 29 (cubic), 70 (tetragonal), and 16 (monoclinic),[21] 18.02 (monoclinic),[40] 33.12 (cubic).[42] Recently, the ionic substitutions in HfO_2, which can enhance the permittivity, have been studied.[45,46]

Although HfO_2 has been widely investigated in recent years due to its important industrial and technological applications, to the best of our knowledge, there have been no systemic studies of the room temperature phase of a monoclinic structure that exists in a wide range of temperatures where it has useful applications. As is well known, optical properties are important because they can be used to determine the optical band gap and electronic dielectric constants. Elastic properties can be used to provide information about interatomic potentials and relate to various fundamental solid state phenomena. Hence, we present first-principles calculations of the

*Project supported by the National Natural Science Foundation of China (Grant Nos. 11347199, 11072225, 10874141, and 10974160), the Specialized Research Fund for Doctoral Program of Higher Education of China (Grant No. 20130184120028), the National Basic Research Program of China (Grant No. 2011CB808201), and the Fundamental Research Funds for the Central Universities, China (Grant Nos. SWJTU112T23 and 2682013CX054).

†Corresponding author. E-mail: qijunliu@home.swjtu.edu.cn

© 2014 Chinese Physical Society and IOP Publishing Ltd

structural, electronic, optical, elastic, mechanical properties and Born effective charges of m-HfO_2.

2. Computational details

Our calculations were performed by the CASTEP code.[47] The geometrical structures and physical properties of m-HfO_2 were calculated within the custom, norm-conserving, and ultrasoft pseudopotential methods based on density functional theory (DFT). We employed the generalized gradient approxiamtion (GGA) with the Perdew–Wang 1991 (PW91) functional[48] for the exchange–correlation energy. For the sampling of Brillouin zone, Monkhorst–Pack scheme k-points samplings (5×5×5) were used for monoclinic structure optimization. The Hf $5d^26s^2$ and O $2s^22p^4$ electrons were explicitly treated as valence electrons and the others were treated as core electrons. The structural optimization is finished until a total energy convergence of 5.0×10^{-6} eV/atom, a maximum force of 0.01 eV/Å, a maximum stress of 0.02 GPa and a maximum displacement of 5.0×10^{-4} Å. During the structure optimizations, this set of parameters could guarantee to achieve a total energy convergence of 5.0×10^{-6} eV/atom, a maximum force of 0.01 eV/Å, a maximum stress of 0.02 GPa, and a maximum displacement of 5.0×10^{-4} Å. Moreover, in order to obtain an accurate bandgap, a hybrid functional PBE0 giving an improved bandgap was used here. The Born effective charges were calculated using the density functional perturbation theory (DFPT), which was implemented in CASTEP.

3. Results and discussion

3.1. Structural properties

In m-HfO_2, there are two symmetry-inequivalent types of O atoms, one is threefold (O_1) and the other is fourfold (O_2) coordinated, owing to the fact that Hf atoms have lattice vectors that are not at right angles any more, nor sevenfold coordinated. We first calculate geometrical structure of m-HfO_2 by minimizing the total energy. The optimized equilibrium lattice parameters are given in Table 1 with the available theoretical[12,17,20,21,24,25,39] and experimental[6] data. It can be seen that the calculated values based on the custom pseudopotential are close to the experimental data. The calculated values based on the ultrasoft and norm-conserving pseudopotential are larger and smaller than experimental values, respectively. The same set (ultrasoft pseudopotential) with plane-wave cutoff energy 380 eV has been used to calculate m-HfO_2, and the parameters $a = 5.315$ Å, $b = 5.414$ Å, $c = 5.452$ Å, and $\beta = 99.615°$ have been obtained.[49] We here use ultrasoft pseudopotential with plane-wave cutoff energy 1000 eV, but the obtained results are very close to the previous results[49] and are also larger than experimental data. According to the best agreement with experimental results, the analyses of electronic structure and optical properties are based on the custom pseudopotential calculations.

Table 1. Calculated structural parameters and their comparisons with available theoretical[12,17,20,21,24,25,39] and experimental[6] data for monoclinic HfO_2. Lattice parameters a, b, c are in Å, β is in degree and V is in $Å^3$. Internal coordinates x, y, and z are dimensionless.

	CASTEP GGA-PW91			Soft Troullier–Martins pseudopotential with LDA[12]	Ultrasoft Vandelbilt pseudopotential with GGA in VASP[17]	Separable Troullier–Martins norm-conserving pseudopotential in SIESTA[20]		Ultrasoft pseudopotential[21]		Norm-conserving nonlocal pseudopotential[24]		Ultrasoft pseudopotential with GGA[25]	Projector augmenyedwave pseudopotential with LDA in VASP[39]	Expt.[6] (average)
	Custom	Ultrasoft	Norm-conserving			DZ	SZ	LDA	GGA	LDA	GGA			
V	35.844	38.822	31.036	–	–	34.3	33.92	34.35	38.01	34.98	36.39	–	–	–
a	5.184	5.327	4.943	5.12	5.133	5.10	5.05	5.106	5.291	5.135	5.215	5.1284	5.029	5.045
b	5.261	5.402	5.009	5.17	5.188	5.17	5.17	5.165	5.405	5.244	5.293	5.1914	5.132	5.190
c	5.339	5.477	5.092	5.29	5.301	5.26	5.27	5.281	5.366	5.269	5.350	5.2969	5.183	5.237
β	100.041	99.806	100.046	–	99.79	99.12	–	99.35	97.92	99.54	99.73	99.71	99.48	99.44
x_{Hf}	0.279	0.279	0.278	0.279				0.280	0.276	0.279	0.277	0.277		0.276
y_{Hf}	0.044	0.042	0.044	0.042				0.043	0.039	0.042	0.042	0.043		0.040
z_{Hf}	0.207	0.207	0.209	0.211				0.209	0.209	0.208	0.207	0.209		0.208
x_{O1}	0.073	0.075	0.071	0.072				0.076	0.089	0.078	0.076	0.074		0.074
y_{O1}	0.341	0.343	0.337	0.340				0.346	0.367	0.350	0.343	0.342		0.339
z_{O1}	0.337	0.338	0.343	0.343				0.337	0.317	0.331	0.335	0.337		0.339
x_{O2}	0.446	0.448	0.451	0.449				0.447	0.447	0.445	0.447	0.448		0.447
y_{O2}	0.759	0.759	0.758	0.758				0.759	0.762	0.760	0.759	0.759		0.753
z_{O2}	0.483	0.484	0.480	0.481				0.483	0.488	0.485	0.483	0.481		0.484

3.2. Electronic properties

Electronic band structure and partial densities of states of m-HfO_2 are shown in Fig. 1 to analyze the electronic structure and chemical bonding. We can see that the maximum of the valence band and the minimum of conduction band are at $\Gamma(G)$ and B points, respectively, and the indirect band gap is 3.296 eV, which is consistent with the previous calculated results 3.7 eV,[3] 3.25 eV,[16] and 3.5 eV.[22] However, these values are all smaller than the experimental data 5.55±0.03,[10] 5.8,[14] 5.56–5.77,[50] and 5.6±0.15[51] due to the well-known band gap underestimation of DFT calculations. The bandgap of PBE0 functional is 6.126 eV, indicating that PBE0 calculations overestimate the bandgap. Table 2 presents the detailed optical transition energies with the valence-to-conduction band transitions. As we can see in Fig. 1, the lower valence bands are mainly derived from the O 2s states; the upper valence bands are dominated by hybridizing O 2p and Hf 5d states, indicating the covalent bonding characteristic in the compound; the lower conduction bands are mostly composed of Hf 5d states as well as small O 2p states, showing the ionic characteristic.

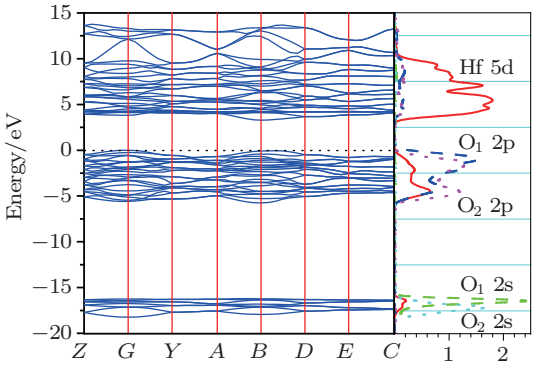


Fig. 1. (color online) Electronic band structure and partial densities of states of m-HfO_2 (The coordinates of the high-symmetry points in Brillouin zone are $Z(0,0,0.5)$, $G(0,0,0)$, $Y(0,0.5,0)$, $A(-0.5,0.5,0)$, $B(-0.5,0,0)$, $D(-0.5,0,0.5)$, $E(-0.5,0.5,0.5)$, $C(0,0.5,0.5)$.

Table 2. Optical transition energies (in eV) and symmetries of the valence-to-conduction band transitions and their comparisons with the available calculated results (in eV)[3,16,22] and experimental band gap (in eV)[10,14,50,51] of m-HfO_2.

Valence-to-conduction band transition	Optical transition energies		Theoretical values	Experimental values
	PW91	PBE0		
$\Gamma \to Z$	3.949	6.825		
$\Gamma \to \Gamma$	3.814	6.595		
$\Gamma \to Y$	4.086	7.037		
$\Gamma \to A$	4.035	6.784		
$\Gamma \to B$	3.296	6.126		
$\Gamma \to D$	3.668	6.465	3.7(GGA),	5.55±0.03[10]
$\Gamma \to E$	3.870	6.677	5.75(sX)[3]	5.8[14]
$\Gamma \to C$	4.086	7.011	3.25[16]	5.56−5.77[50]
$Z \to Z$	4.441	7.362	3.5[22]	5.6±0.15[51]
$Y \to Y$	4.652	7.698		
$A \to A$	4.719	7.510		
$B \to B$	3.395	6.228		
$D \to D$	4.149	7.019		
$E \to E$	4.668	7.569		
$C \to C$	4.798	7.825		

The Mulliken charges are calculated to understand the nature of chemical bonding. The Mulliken charges are determined to be +1.36 e for Hf atoms, $-0.65e$ and $-0.71e$ for O_1 and O_2 atoms, indicating that the electron transfer from Hf atoms to O_1/O_2 atoms is 0.65 e/0.71 e. Here, we use the effective valence defined as the difference between the Mulliken charge and the formal ionic charge on the cation species[52] to analyze the Hf–O bonding. The effective valence of Hf cation is +2.64, which is larger than zero, indicating that there is mainly covalent bonding in m-HfO_2. Figure 2 shows the electronic charge densities from (a) (200), (b) (400), and (c) (004) planes of m-HfO_2. We can see that charge densities around O atoms in (200) plane are almost symmetric and the weak covalent interactions occur between neighboring O atoms. From the (400) and (004) planes, the covalent characteristic of Hf–O bonding is shown. In particular, the anisotropic charge densities around O atoms in (004) plane, which point to neighboring Hf atoms, further approve the covalent characteristic.

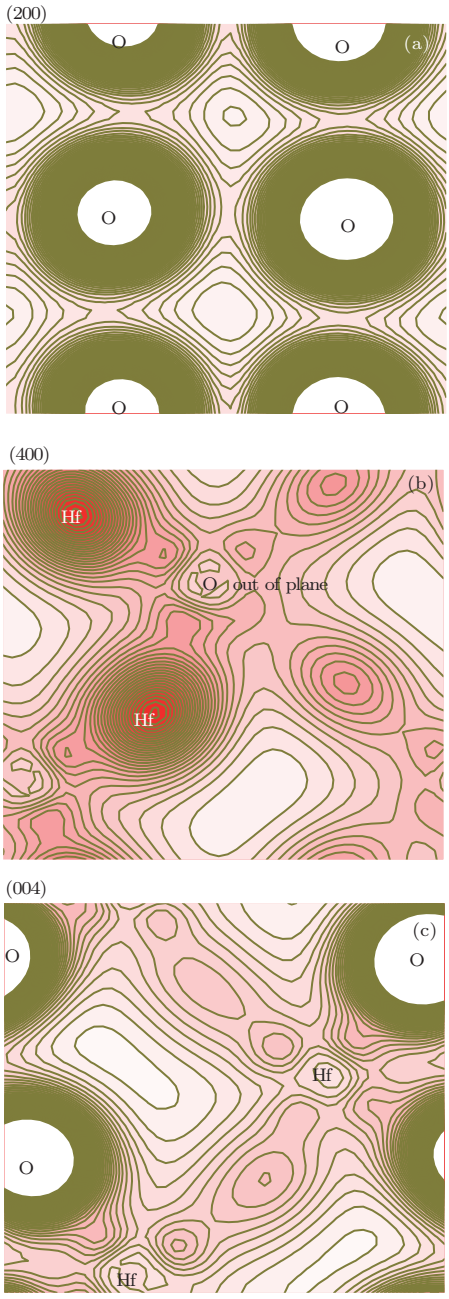


Fig. 2. (color online) Electronic charge densities from (a) (200), (b) (400), and (c) (004) planes of m-HfO_2.

3.3. Optical properties

The optical properties are determined from the frequency-dependent dielectric function $\varepsilon(\omega) = \varepsilon_1(\omega) + i\varepsilon_2(\omega)$, which is mainly contributed from the electronic structure. The imaginary part that shows the real transitions between the occupied and unoccupied wave functions is given as follows:[53,54]

$$\varepsilon_2(\omega) = \left(\frac{4\pi^2 e^2}{m^2\omega^2}\right)\sum_{i,j}\int \langle i|M|j\rangle^2 f_i(1-f_i) \times \delta(E_f - E_i - \omega)\,\mathrm{d}^3k, \quad (1)$$

where M is the dipole matrix, i and j are the initial and final states, f_i is the Fermi distribution function for the i-th state, and E_i is the energy of electron in the i-th state. The real part $\varepsilon_1(\omega)$ of the dielectric function can be calculated using the Kramers–Kroning relations:[53,54]

$$\varepsilon_1(\omega) = 1 + \frac{2}{\pi}P\int_0^{\infty}\frac{\omega'\varepsilon_2(\omega')\,\mathrm{d}\omega'}{(\omega'^2 - \omega^2)}, \quad (2)$$

where P is the principal value of the integral

$$\left(P = \lim_{a\to 0}\int_{-\infty}^{\omega-a}\frac{\varepsilon(\omega')}{\omega'-\omega}\,\mathrm{d}\omega' + \lim_{a\to 0}\int_{\omega+a}^{+\infty}\frac{\varepsilon(\omega')}{\omega'-\omega}\,\mathrm{d}\omega'\right).$$

Other optical properties, such as refractive index $n(\omega)$, extinction coefficient $k(\omega)$, reflectivity $R(\omega)$, absorption coefficient $I(\omega)$, loss function $L(\omega)$, and optical conductivity $\sigma(\omega)$ can be obtained from $\varepsilon(\omega)$ as[53,54]

$$n(\omega) = \left[\frac{\varepsilon_1(\omega)}{2} + \frac{\sqrt{\varepsilon_1(\omega)^2 + \varepsilon_2(\omega)^2}}{2}\right]^{1/2}, \quad (3)$$

$$k(\omega) = \left[\frac{\sqrt{\varepsilon_1(\omega)^2 + \varepsilon_2(\omega)^2}}{2} - \frac{\varepsilon_1(\omega)}{2}\right]^{1/2}, \quad (4)$$

$$R(\omega) = \left|\frac{\varepsilon^{1/2}(\omega) - 1}{\varepsilon^{1/2}(\omega) + 1}\right|^2, \quad (5)$$

$$I(\omega) = \sqrt{2}(\omega)\left(\sqrt{\varepsilon_1(\omega)^2 + \varepsilon_2(\omega)^2} - \varepsilon_1(\omega)\right)^{1/2}, \quad (6)$$

$$L(\omega) = -Im\left(\frac{1}{\varepsilon(\omega)}\right) = \frac{\varepsilon_2(\omega)}{\varepsilon_1^2(\omega) + \varepsilon_2^2(\omega)}, \quad (7)$$

$$\sigma(\omega) = \sigma_1(\omega) + i\sigma_2(\omega) = -i\frac{\omega}{4\pi}[\varepsilon(\omega) - 1]. \quad (8)$$

The imaginary and real parts of the complex dielectric function for m-HfO_2, as well as the experimental data,[55] are shown in Fig. 3, where we can see that our calculated results are in good agreement with the experimental data (a scissors operator is used to deal with the underestimated band gap[56]). The peaks of $\varepsilon_2(\omega)$ in Fig. 3 arise mainly from the electron transitions between O 2p and Hf 5d. Moreover, the obvious optical anisotropy of m-HfO_2 is found to be due to the monoclinic structure. The calculated electronic parts of the static dielectric constants are 3.991, 3.931, and 3.638 for ε_{xx}, ε_{yy}, and ε_{zz}, respectively.

The calculated values of refractive index, extinction coefficient, optical reflectivity, absorption coefficient, energy-loss function, and complex conductivity function of m-HfO_2 are shown in Fig. 4. The calculated values of static refractive index are 1.998, 1.983, and 1.907 for n_{xx}, n_{yy}, and n_{zz}, respectively, which are in good agreement with the experimental data.[9,15,50] Our results for the static dielectric constant and static refractive index satisfy the relation $n(0) = \sqrt{\varepsilon(0)}$ at low frequency, indicating that our results are reasonable. The reflectivity is lower than 20% from 0 to 5.7 eV, indicating that m-HfO_2 is of transmission for frequencies in this range. When the electromagnetic wave passes through a material, the fraction of energy lost

means the absorption coefficient of the material. The absorption coefficient starts at 5.7 eV and then increases, which is consistent with the optical band gap. The peaks of the energy-loss function are associated with the plasma resonance, and the corresponding frequency is named bulk plasma frequency $\omega(p)$, which shows the transition from metallic behavior [$\varepsilon_1(\omega) < 0$] to dielectric behavior [$\varepsilon_1(\omega) > 0$]. The calculated plasma frequencies are 21.747, 21.987, and 21.713 eV for L_{xx}, L_{yy}, and L_{zz}, respectively, which correspond to the abrupt reduction of reflectivity. The complex conductivity function is the absorptive $\sigma_1(\omega)$ and reactive $\sigma_2(\omega)$ current response to a time-varying external electrical field of frequency, and the origins of the peaks in $\varepsilon_2(\omega)$ can explain the occurrences of the peaks in $\sigma_1(\omega)$.

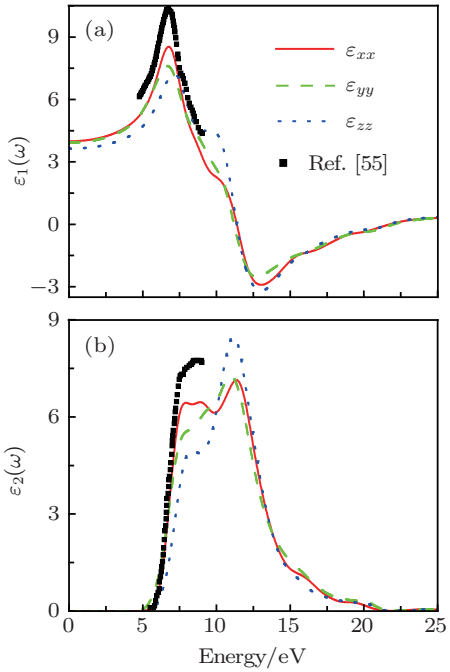


Fig. 3. (color online) Real (upper panel) and imaginary (lower panel) parts of complex dielectric function for m-HfO_2 as well as the experimental data.[55]

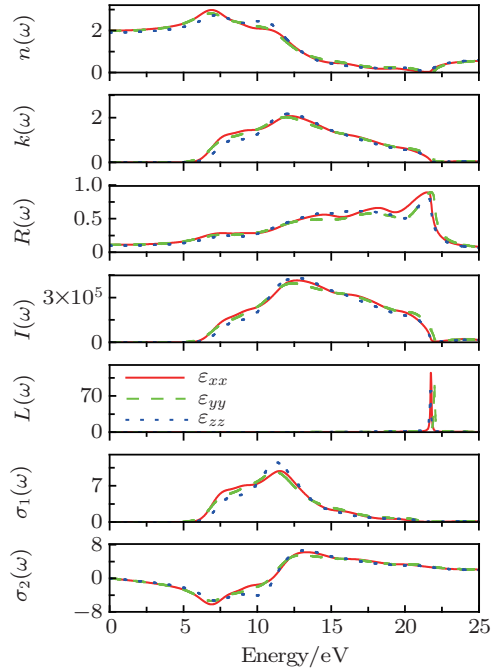


Fig. 4. (color online) Plots of refractive index $n(\omega)$, extinction coefficient $k(\omega)$, reflectivity $R(\omega)$, absorption coefficient $I(\omega)$, loss function $L(\omega)$, and optical conductivity $\sigma(\omega)$ versus energy of m-HfO_2.

3.4. Elastic and mechanical properties

The elastic constants are important to understand the response to an applied macroscopic stress, which are defined by means of a Taylor expansion of the total energy. The energy of a strained system is expressed as follows:[57–59]

$$U(V,\varepsilon) = U(V_0,0) + V_0\left[\sum_i \tau_i\varepsilon_i\xi_i + \frac{1}{2}\sum_{ij} C_{ij}\varepsilon_i\xi_i\varepsilon_j\xi_j\right], \quad (9)$$

where $U(V_0,0)$ is the energy of the unstrained system with equilibrium volume V_0, τ_i is an element in the stress tensor, and ξ_i is a factor to take the Voigt index into consideration. The calculated thirteen independent components of m-HfO_2 and the available data[60] are shown in Table 3. As is well known, the conditions of mechanical stability are important to estimate a stable compound. Hence, the calculated elastic constants of m-HfO_2 should satisfy the Born stability criteria:[61,62]

$$\begin{aligned}
&C_{11} > 0, \quad C_{22} > 0, \quad C_{33} > 0,\\
&C_{44} > 0, \quad C_{55} > 0, \quad C_{66} > 0,\\
&(C_{11}+C_{22}+C_{33}+2C_{12}+2C_{13}+2C_{23}) > 0,\\
&(C_{33}C_{55}-C_{35}^2) > 0, \quad (C_{44}C_{66}-C_{46}^2) > 0,\\
&(C_{22}+C_{33}-2C_{23}) > 0,\\
&[C_{22}(C_{33}C_{55}-C_{35}^2)+2C_{23}C_{25}C_{35}-C_{23}^2C_{55}-C_{25}^2C_{33}] > 0,\\
&\{2[C_{15}C_{25}(C_{33}C_{12}-C_{13}C_{23})+C_{15}C_{35}(C_{22}C_{13}-C_{12}C_{23})\\
&+C_{25}C_{35}(C_{11}C_{23}-C_{12}C_{13})]-[C_{15}^2(C_{22}C_{33}-C_{23}^2)\\
&+C_{25}^2(C_{11}C_{33}-C_{13}^2)+C_{35}^2(C_{11}C_{22}-C_{12}^2)]\\
&+C_{55}(C_{11}C_{22}C_{33}-C_{11}C_{23}^2-C_{22}C_{13}^2\\
&-C_{33}C_{12}^2+2C_{12}C_{13}C_{23})\} > 0. \qquad (10)
\end{aligned}$$

It can be seen that the elastic constants satisfy the inequalities in Eq. (10), which shows that m-HfO_2 is mechanically stable.

Voigt[63] proposed the average of relations expressing the stress in terms of the given strain. Reuss and Angew[64] proposed the average of relations expressing the strain in terms of the given stress. Hill[65] proved that the approximations made by Voigt and Reuss represent the upper and lower bounds of elastic constants, respectively.

Table 3. Calculated independent elastic constants (in GPa) and the available theoretical data for m-HfO_2.

Elasticity	C_{11}	C_{22}	C_{33}	C_{12}	C_{13}	C_{23}	C_{44}	C_{55}	C_{66}	C_{15}	C_{25}	C_{35}	C_{46}
This work	336.66	428.20	195.25	234.56	143.33	123.02	120.28	73.81	145.56	64.41	23.47	56.75	–13.13
Ref. [60]	340.9	392.8	288.2	164.4	107	158.6	86.9	93.5	131.5	41.9	–8.4	–0.4	–9.9

Table 4. Calculated values of bulk modulus B, shear modulus G, Young's modulus E (in GPa), B/G, Poisson's ratio, compressibility (in GPa^{-1}), and Lamé constants (in GPa).

B_X			$G_X(\mu_X)$			B_X/G_X			E_X		
$X=R$	$X=V$	$X=H$	$X=R$	$X=V$	$X=H$	$X=R$	$X=V$	$X=H$	$X=R$	$X=V$	$X=H$
137.74	217.99	177.87	74.06	98.54	86.30	1.860	2.212	2.061	188.41	257.03	222.86
251,[12] 254 (DZ) and 296 (SZ),[20] 192 (GGA) and 186 (LDA),[24] 215 (LDA) and 152 (GGA),[25] 185 (DAC+ADX) and 168 (GGA),[60] 235,[66] 233.1,[6] 284,[67] 145[23]			98.7,[60] 120,[66] 100–110[6]			–			200–250[6]		
ν_X			β_X ($\times 10^{-3}$)			λ_X					
$X=R$	$X=V$	$X=H$	$X=R$	$X=V$	$X=H$	$X=R$	$X=V$	$X=H$			
0.272	0.304	0.291	7.26	4.59	5.62	88.37	152.30	120.33			
0.25–0.30[6]			–			–					

These equations are shown as

$$B_{\text{Voigt}} = \frac{1}{9}(C_{11}+C_{22}+C_{33})+\frac{2}{9}(C_{12}+C_{13}+C_{23}), \quad (11)$$

$$G_{\text{Voigt}} = \frac{1}{15}(C_{11}+C_{22}+C_{33}-C_{12}-C_{13}-C_{23}) + \frac{1}{5}(C_{44}+C_{55}+C_{66}), \quad (12)$$

$$B_{\text{Reuss}} = [(S_{11}+S_{22}+S_{33})+2(S_{12}+S_{13}+S_{23})]^{-1}, \quad (13)$$

$$G_{\text{Reuss}} = 15[4(S_{11}+S_{22}+S_{33})-4(S_{12}+S_{13}+S_{23}) + 3(S_{44}+S_{55}+S_{66})]^{-1}, \quad (14)$$

$$B_{\text{Hill}} = \frac{1}{2}(B_{\text{Reuss}}+B_{\text{Voigt}}), \quad (15)$$

$$G_{\text{Hill}} = \frac{1}{2}(G_{\text{Reuss}}+G_{\text{Voigt}}), \quad (16)$$

where the S_{ij} is the inverse matrix of the elastic constant matrix C_{ij} and the relations between S_{ij} and C_{ij} are shown in Ref. [57]. The Young's modulus, Poisson's ratio, and Lamé constants can then be computed by the following equations:

$$E_X = \frac{9B_XG_X}{G_X+3B_X}, \quad (17)$$

$$\nu_X = \frac{1}{2}\left[\frac{B_X-(2/3)G_X}{B_X+(1/3)G_X}\right], \quad (18)$$

$$\mu_X = E_X/[2(1+\nu_X)], \quad (19)$$

$$\lambda_X = \nu_X E_X/[(1+\nu_X)(1-2\nu_X)], \quad (20)$$

where X is Voigt, or Reuss, or Hill.

The calculated results of mechanical properties are presented in Table 4, along with the available theoretical[12,20,24,25,60,66] and experimental data.[6,23,67] The calculated bulk modulus of m-HfO_2 is 177.87 GPa, which is lower than the experimental data 233.1 GPa[6] and 284 GPa,[67] and is larger than the value of 145 GPa.[23] As is well known, the bulk modulus and shear modulus represent the resistance to fracture and the resistance to plastic deformation, respectively, and a high (low) ratio of bulk to shear modulus (B/G) value is associated with ductility (brittleness). The critical value of the ductile–brittle transition is 1.75.[68] Our obtained value is 2.061, indicating that m-HfO_2 exhibits high shear deformation resistance and behaves in a ductile manner.

The Debye temperature, which is related to the solid sound velocity and atomic vibration frequency, can be estimated from the average sound velocity:[58]

$$\Theta = \frac{h}{k}\left(\frac{3nN\rho}{4\pi M}\right)^{1/3}\upsilon_m, \quad (21)$$

where h is the Planck's constant, k the Boltzmann's constant, n the number of atoms in unit cell, N the Avogadro's number, ρ the density, M the molecular mass, and υ_m is the average sound velocity, which is obtained from Ref. [58]

$$\upsilon_m = [(2/\upsilon_s^3+1/\upsilon_p^3)/3]^{-1/3}, \quad (22)$$

where υ_s and υ_p are the shear and compressional sound velocity, respectively, which are defined as follows:[58]

$$\upsilon_s = \sqrt{G_X/\rho}, \quad (23)$$

$$\upsilon_p = \sqrt{(B_X+4G_X/3)/\rho}. \quad (24)$$

We obtain the Debye temperature 431 K of m-HfO_2 shown in Table 5, which is smaller than the value 483 K of the polycrystal HfO_2 with SIESTA-GGA calculation.[69] As is well known, the Debye temperature is associated with thermal conductivity according to the rule of thumb. Hence, compared with polycrystal HfO_2, m-HfO_2 shows a relatively soft lattice and bad thermal conductivity.

Table 5. Calculated values of the shear, compressional, average sound velocity, and Debye temperature.

v_s^X/(m/s)			v_p^X/(m/s)		
$X=R$	$X=V$	$X=H$	$X=R$	$X=V$	$X=H$
2728	3146	2944	4874	5924	5425
v_m^X/(m/s)			Θ/K		
$X=R$	$X=V$	$X=H$	$X=R$	$X=V$	$X=H$
3037	3516	3285	398	461	431

3.5. Born effective charges

The Born effective charge tensor for the β component has been obtained as[70]

$$Z^*_{i,\alpha\beta} = \frac{V}{|e|}\frac{(\Delta P)_\alpha}{\Delta u}, \tag{25}$$

where $Z^*_{i,\alpha\beta}$ is the Born effective charge tensor, Δu is the displacement of the i-th atom in the unit cell, ΔP is the total difference in polarization, V is the volume of the unit cell, and α is the direction of the polarization. The calculated Born effective charges of m-HfO_2 are shown in Table 6, where we can see that the Born effective charges are consistent with the values given in Ref. [21] and show different characteristic due to the symmetry. As is well known, Born effective charges show an estimate of the charge transfer linearly caused by a unit sublattice displacement.[71] The nominal ionic charges of Hf and O are +4 and −2, respectively. However, the absolute values of Born effective charges of Hf and O are larger than their absolute values of nominal charges, indicating that there is mainly a covalent bond in m-HfO_2.

Table 6. Calculated Born effective charges of monoclinic HfO_2.

	Hf			O_1			O_2		
	GGA	Ref. [21]		GGA	Ref. [21]		GGA	Ref. [21]	
		LDA	GGA		LDA	GGA		LDA	GGA
xx	5.95	5.56	5.57	–3.23	–3.09	–3.10	–2.72	–2.48	–2.47
xy	–0.24	–0.47	–0.56	1.12	0.97	0.90	0.26	0.20	0.15
xz	0.19	0.96	0.91	–0.08	–0.58	–0.53	–0.12	–0.39	–0.36
yx	–0.32	–0.13	–0.02	0.93	1.37	1.29	0.15	0.21	0.11
yy	5.89	5.55	5.57	–2.74	–2.73	–2.70	–3.14	–2.82	–2.87
yz	0.56	0.14	0.07	–0.82	–0.71	–0.61	0.59	0.35	0.40
zx	0.18	0.21	0.27	–0.18	–0.18	–0.20	0.00	–0.07	–0.09
zy	0.28	0.41	0.45	–0.92	–0.61	–0.51	0.46	0.43	0.46
zz	5.10	4.74	4.64	–2.26	–2.24	–2.16	–2.84	–2.58	–2.52

4. Conclusions

In this paper, we investigated the structural, electronic, optical, elastic, mechanical properties, and Born effective charges of m-HfO_2. Our calculated lattice constants are in agreement with other experimental and theoretical data. The electronic structure and density of states calculations show an indirect band gap Γ–B and a hybridization between Hf 5d and O 2p states. The calculated dielectric function shows that it is consistent with the experimental results and presents optically anisotropic behavior. Elastic and mechanical properties are obtained, which show that m-HfO_2 is mechanically stable, exhibits high shear deformation resistance, and behaves in a ductile manner.

References

[1] Zheng X H, Huang A P, Yang Z C, Xiao Z S, Wang M and Cheng G A 2011 *Acta Phys. Sin.* **60** 017702 (in Chinese)
[2] Monaghan S, Hurley P K, Cherkaoui K, Negara M A and Schenk A 2009 *Solid State Electron.* **53** 438
[3] Xiong K and Robertson J 2005 *Microelectron. Eng.* **80** 408
[4] Zhu S Y, Xu J P, Wang L S and Huang Y 2013 *Chin. Phys. B* **22** 097301
[5] Xiong K, Robertson J, Gibson M C and Clark S J 2005 *Appl. Phys. Lett.* **87** 183505
[6] Wang J, Li H P and Stevens R 1992 *J. Mater. Sci.* **27** 5397, and the references therein
[7] Wang J, Ponton C B and Marouis P M 1994 *J. Mater. Sci.* **29** 3577
[8] Ohtaka O, Fukui H, Kunisada T, Fujisawa T, Funakoshi K, Utsumi W, Irifune T, Kuroda K and Kikegawa T 2001 *J. Am. Ceram. Soc.* **84** 1369
[9] Franta D, Ohlídal I, Nečas D, Vižd'a F, Caha O, Hasoň M and Pokorný P 2011 *Thin Solid Films* **519** 6085
[10] Aarik J, Mändar H, Kirm M and Pung L 2004 *Thin Solid Films* **466** 41
[11] Mergia K, Liedtke V, Speliotis Th, Apostolopoulos G and Messoloras S 2009 *Adv. Mater. Res.* **59** 87
[12] Lowther J E, Dewhurst J K, Leger J M and Haines J 1999 *Phys. Rev. B* **60** 14485
[13] Mirgorodsky A P and Quintard P E 1999 *J. Am. Ceram. Soc.* **82** 3121
[14] Robertson J 2006 *Rep. Prog. Phys.* **69** 327
[15] Pereira L, Barquinha P, Fortunato E and Martins R 2006 *Mater. Sci. Semicond. Proc.* **9** 1125
[16] Chen W, Sun Q Q, Ding S J, Zhang D W and Wang L K 2006 *Appl. Phys. Lett.* **89** 152904
[17] Hou Z F, Gong X G and Li Q 2008 *J. Phys.: Condens. Matter* **20** 135206
[18] Chen T J and Kuo C L 2011 *J. Appl. Phys.* **110** 064105
[19] Terki R, Bertrand G, Aourag H and Coddet C 2008 *Mater. Lett.* **62** 1484
[20] Caravaca M A and Casali R A 2005 *J. Phys.: Condens. Matter* **17** 5795
[21] Zhao X and Vanderbilt D 2002 *Phys. Rev. B* **65** 233106
[22] Perevalov T V, Gritsenko V A, Erenburg S B, Badalyan A M, Wong H and Kim C W 2007 *J. Appl. Phys.* **101** 053704
[23] Leger J M, Atouf A, Tomaszewski P E and Pereira A S 1993 *Phys. Rev. B* **48** 93
[24] Kang J, Lee E C and Chang K J 2003 *Phys. Rev. B* **68** 054106
[25] Jaffe J E, Bachorz R A and Gutowski M 2005 *Phys. Rev. B* **72** 144107
[26] Tang C and Ramprasad R 2010 *Phys. Rev. B* **81** 161201(R)

[27] Kirsch P D, Quevedo-Lopez M A, Li H J, Senzaki Y, Peterson J J, Song S C, Krishnan S A, Moumen N, Barnett J, Bersuker G, Hung P Y, Lee B H, Lafford T, Wang Q, Gay D and Ekerdt J G 2006 *J. Appl. Phys.* **99** 023508

[28] Kukli K, Ritala M, Pilvi T, Aaltonen T, Aarik J, Lautala M and Leskelä M 2005 *Mater. Sci. Eng. B* **118** 112

[29] Zhang L S and Xu H 2008 *High Power Laser Particle Beams* **20** 894 (in Chinese)

[30] Lucovsky G, Seo H, Fleming L B, Lüning J, Lysaght P and Bersuker G 2007 *Surf. Sci.* **601** 4236

[31] Chen G H, Hou Z F and Gong X G 2008 *Comput. Mater. Sci.* **44** 46

[32] Lu H L, Xu M, Chen W, Ren J, Ding S J and Zhang W 2006 *Acta Phys. Sin.* **55** 1374 (in Chinese)

[33] Tuttle B R, Tang C G and Ramprasad R 2007 *Phys. Rev. B* **75** 235324

[34] Shin M, Park Y, Kong K J and Chang H 2011 *Appl. Phys. Lett.* **98** 173501

[35] Gavartin J L and Shluger A L 2007 *Microelectron. Eng.* **84** 2412

[36] Wang W, Gong C, Shan B, Wallace R M and Cho K 2011 *Appl. Phys. Lett.* **98** 232113

[37] Scheidecker R W, Hunter O Jr and Calderwood F W 1979 *J. Mater. Sci.* **14** 2284

[38] de Boer P K and de Groot R A 1998 *J. Phys.: Condens. Matter* **10** 10241

[39] Luo X, Zhou W, Ushakov S V, Navrotsky A and Demkov A A 2009 *Phys. Rev. B* **80** 134119

[40] Silva C C, Leite Alves H W and Scolfaro L M R 2007 *AIP Conf. Proc.* **893** 311

[41] Jiang H, Gomez-Abal R I, Rinke P and Scheffler M 2010 *Phys. Rev. B* **81** 085119

[42] Debernardi A and Fanciulli M 2006 *Mater. Sci. Semicond. Proc.* **9** 1014

[43] Muñoz Ramo D, Gavartin J L, Shluger A L and Bersuker G 2007 *Microelectron. Eng.* **84** 2362

[44] Weng H M and Dong J M 2006 *Phys. Rev. B* **73** 132410

[45] Zhang W, Chen W Z, Sun J Y and Jiang Z Y 2013 *Chin. Phys. B* **22** 016601

[46] Dutta G 2009 *Appl. Phys. Lett.* **94** 012907

[47] Clark S J, Segall M D, Pickard C J, Hasnip P J, Probert M J, Refson K and Payne M C 2005 *Z. Kristallogr.* **567** 220

[48] Perdew J P, Chevary J A, Vosko S H, Jackson K A, Pederson M R, Singh D J and Fiolhais C 1992 *Phys. Rev. B* **46** 6671

[49] Liu Q J, Liu Z T and Feng L P 2011 *Adv. Mater. Res.* **216** 341

[50] He G, Zhu L Q, Liu M, Fang Q and Zhang L D 2007 *Appl. Surf. Sci.* **253** 3413

[51] Afanasév V V, Stesmans A, Chen F, Shi X and Campbell S A 2002 *Appl. Phys. Lett.* **81** 1053

[52] Segall M D, Shah R, Pickard C J and Payne M C 1996 *Phys. Rev. B* **54** 16317

[53] Shen X C 1992 *Semiconductor Spectroscopy and Optical Properties*, 2nd edn. (Beijing: Science Press) p. 76 (in Chinese)

[54] Okoye C M I 2003 *J. Phys.: Condens. Matter* **15** 5945, and the references therein

[55] Lim S G, Kriventsov S, Jackson T N, Haeni J H, Schlom D G, Balbashov A M, Uecker R, Reiche P, Freeouf J L and Lucovsky G 2002 *J. Appl. Phys.* **91** 4500

[56] Asahi R, Taga Y, Mannstadt W and Freeman A J 2000 *Phys. Rev. B* **61** 7459

[57] Chen H S 1996 *Elastic Anisotropy of Metal* (Beijing: Metallurgy Industry Press) p. 20 (in Chinese)

[58] Tian S 2004 *Materials Physical Properties* (Beijing: Beijing University of Aeronautics and Astronautics Press) p. 379 (in Chinese)

[59] Fast L, Wills J M, Johansson B and Eriksson O 1995 *Phys. Rev. B* **51** 17431

[60] Al-Khatatbeh Y, Lee K K M and Kiefer B 2010 *Phys. Rev. B* **82** 144106

[61] Born M and Huang K 1954 *Dynamical Theory of Crystal Lattices* (Oxford: Clarendon) p. 82

[62] Wu Z J, Zhao E J, Xiang H P, Hao X F, Liu X J and Meng J 2007 *Phys. Rev. B* **76** 054115

[63] Voigt W 1928 *Lehrbuch der Kristallphysik* (Leipzig: Teubner) p. 574

[64] Reuss A 1929 *Z. Angew. Math. Mech.* **9** 49

[65] Hill R 1952 *Proc. Phys. Soc. Lond.* **65** 349

[66] Shan T R, Devine B D, Kemper T W, Sinnott S B and Phillpot S R 2010 *Phys. Rev. B* **81** 125328

[67] Desgreniers S and Lagarec K 1999 *Phys. Rev. B* **59** 8467

[68] Pugh S F 1954 *Philos. Mag.* **45** 823

[69] Caravaca M A, Miño J C, Pérez V J, Casali R A and Ponce C A 2009 *J. Phys.: Condens. Matter* **21** 015501

[70] Shi S Q, Ke X Z, Zhang H, Ouyang C Y, Lei M S and Chen L Q 2009 *Phys. Lett. A* **373** 4096

[71] Labat F, Baranek P, Domain C, Minot C and Adamo C 2007 *J. Chem. Phys.* **126** 154703